

The background image shows two men in white lab coats or shirts working in a laboratory. They are focused on a blue, multi-tiered apparatus on a table. A yellow tube is connected to the top of the apparatus. The setting appears to be a modern research facility with large windows in the background.

SAG Foam EOR
The Impact of Grid
Refinement on Gas
and Liquid
Injectivity during
SAG Foam EOR

Lily Qian

SAG Foam EOR
The Impact of Grid Refinement on
Gas and Liquid Injectivity during
SAG Foam EOR

by

L. Qian

to obtain the degree of

Bachelor of Science

at the Delft University of Technology,

to be defended publicly on Thursday July 5, 2018 at 3:30 PM.

Student Number:	4766059
Project Duration:	April 11 th , 2018 – July 5 th , 2018
Thesis committee:	Prof. dr. ir. W. Rossen, TU Delft, supervisor
	MSc. ir. R. Salazar, TU Delft
	Dr. ir. A.C. Dieudonné, TU Delft

An electronic version of this thesis is available at <http://repository.tudelft.nl/>

Abstract

Surfactant-Alternating-Gas (SAG) is a popular enhanced oil recovery method that utilizes foam to decrease gas mobility and subsequently improve reservoir sweep efficiency. SAG is known to have many benefits, such as mitigating corrosion effects and increasing gas injectivity. Despite this, liquid injectivity is typically very poor during the SAG process. Currently, there is not a consistent model for liquid injectivity during SAG. However, Gong et al. recently conducted core-flood experiments to gain clarity on how gas and liquid injectivity are affected during SAG in near-wellbore conditions. Gong et al. determined that gas and liquid injectivity are represented by the propagation of multiple banks. For gas injectivity, there are two banks: the collapsed-foam bank and the foam bank. For liquid injectivity, there are three banks: the collapsed-foam bank, the gas dissolution bank and the liquid-fingering bank.

Conventional foam simulators, such as CMG's STARS, use the Peaceman equation to obtain an estimate for well pressure as well as liquid and gas injectivity. Gong et al. came to the conclusion that conventional foam simulators do not take the propagation of the collapsed-foam bank into account. Thus, Gong et al.'s results indicate that the Peaceman equation greatly underestimates gas and liquid injectivity during SAG in a 100 by 100 meter grid block. Subsequently, this paper aims to determine how refining the 100 by 100 meter grid block will alter well pressure and liquid and gas injectivity, especially in the near-wellbore region.

We used CMG's STARS, a conventional foam simulator, to test the impact of grid refinement on injectivity and well block pressure. Our grid set-ups include a base grid of 5x5 equal blocks and two refined grid cases, in which the center grid blocks are partitioned into 9 and 25 equal block pieces. Our results indicate that as we refine the grid, the dimensionless pressure drops occur quicker and the magnitude of pressure decreases. When compared to the base grid, the pressure drops of the refined grids were discovered to be approximately 9 and 25 times faster for the 3x3 center grid case and the 5x5 center grid case respectively. Additionally, we observed additional dimensionless pressure peaks in the refined cases, which can be explained by a drop in relative mobility when the foam reaches a new grid block.

Although our foam parameters were based on Gong et al.'s foam scan, our foam parameters are not exactly the same as the parameters listed in Gong et al.'s paper because we did not include foam shear-thinning properties. In order to build on this paper's research, future research should look into comparing our STAR's results to the fractional-flow theory. Additionally, future models and research should look into reducing the simulation's time step in order to increase the number of iterations calculated by the simulator, especially around the region in which the pressure drop occurs. Lastly, it would also be important to look into finding the best method to represent the well block pressure for a refined grid case.

Contents

Tables of Figures.....	5
Introduction.....	6
Background and Theory.....	8
2.1. Gong et al.'s Summary of Results	8
2.1.1. Gong et al.'s Laboratory Experiment.....	8
2.1.2. Linear-flow Model	9
2.1.3. Radial-flow Model	10
2.1.4. Conventional Foam Simulation	10
2.1.5. The Peaceman Equation.....	10
2.1.6. Gong et al.'s Assumptions	11
2.1.7. Comparison between Radial-flow Model and Peaceman Equation.....	11
2.2. STARS Foam Modelling	12
Methodology	14
3.1 The Grid Models	14
3.2 General Parameters	15
3.3 Relative Permeability Parameters	16
3.4 Foam Parameters.....	17
Results.....	19
4.1 Dimensionless Pressure	19
4.2 Comparison of Pressures along the Grid's Diagonal.....	23
Conclusion and Recommendations.....	27
References.....	28

Tables of Figures

Figure 1. Gas injection foam banks (Gong et al., 2018).....	8
Figure 2. Liquid injection banks (Gong et al., 2018).....	8
Figure 3. Pressure gradient comparison during gas injection (Gong et al., 2018).....	9
Figure 4. Pressure gradient comparison during liquid injection following 135 TPV of gas injection (Gong et al., 2018).	10
Figure 5. Dimensionless pressure drop during gas injection for Peaceman equation and radial-flow model (Gong et al., 2018).	11
Figure 6. Dimensionless pressure drop during liquid injection for Peaceman equation and radial-flow model (Gong et al., 2018).	12
Figure 7. Base case: 5x5x1 grid	14
Figure 8. Refined grid: 3x3 Center	15
Figure 9. Refined grid: 5x5 Center	15
Figure 10. Foam Apparent Viscosity vs. Foam Gas Fraction (Gong et al., 2018).	18
Figure 11. Original Grid: Dimensionless Pressure vs. PV Injected after gas injection	20
Figure 12. Original Grid: Dimensionless Pressure vs. PV Injected after liquid injection	20
Figure 13. Refined 3x3 Grid: Dimensionless Pressure vs. PV Injected after gas injection.....	21
Figure 14. Refined 3x3 Grid: Dimensionless Pressure vs. PV Injected after liquid injection.	21
Figure 15. Refined 5x5 Grid: Dimensionless Pressure vs. PV Injected after gas injection.....	22
Figure 16. Refined 5x5 Grid: Dimensionless Pressure vs. PV Injected after liquid injection.	22
Figure 17. Pressure notation along the grid block diagonal.....	23
Figure 18. Original Grid: Diagonal pressures during gas injection	24
Figure 19. Original Grid: Diagonal pressures during liquid injection	24
Figure 20. Refined 3x3 Grid: Diagonal pressures during gas injection.....	25
Figure 21. Refined 3x3 Grid: Diagonal pressures during liquid injection.....	25
Figure 22. Refined 5x5 Grid: Diagonal pressures during gas injection.....	26
Figure 23. Refined 5x5 Grid: Diagonal pressures during liquid injection.....	26

1

Introduction

Primary oil recovery only recovers approximately 30 percent of the original hydrocarbons in place (Terry, 2003). As a result, many operators utilize tertiary recovery methods, or enhanced oil recovery (EOR), to gain access to the remaining reserves. Enhanced oil recovery incorporates any recovery process that extends beyond using the resources, such as water and gas, that are already present within the formation (Lake, 1989). Injecting foams into the formation is a common tactic in enhanced oil recovery. Since gases tend to have low viscosities and reservoirs are typically very heterogeneous, the sweep efficiency of injected gas is very low (Rossen, 1996; Shan & Rossen, 2004). However, foam can be used to combat the effects of reservoir heterogeneity and reduce gas mobility, thereby increasing sweep efficiency. Additionally, foam does not affect water and oil viscosity nor change the relative permeability function for water (Renkema & Rossen, 2007).

Foams used in EOR are fluids made up of gas bubbles separated by surfactant-stabilized liquid films, called lamellae. The two main applications of foam include plugging unproductive reservoir layers near the well and redirecting flow patterns in order to significantly increase foam propagation and oil recovery (Rossen, 1996). Continuous-gas foam readily facilitates gas flow in a porous media whereas discontinuous-gas foam is filled with foam films that obstruct all gas flow pathways. There are two primary foam injection methods. The first method incorporates injecting liquid and gas slugs simultaneously and continuously and is generally used in steam-flood operations. The second method, known as surfactant-alternating gas (SAG), consists of alternating injections of foam and gas slugs (Renkema & Rossen, 2007; Rossen, 1996). The main advantages of using SAG include reducing corrosion in pipes and surface facilities (especially for CO₂ foam injection) and increasing gas injectivity. As a result, the SAG process is typically the preferred method of foam injection (Gong et al., 2018).

Although the SAG process has good benefits, poor liquid injectivity is one of the negative side effects of SAG foam applications. Conventional foam simulators use the Peaceman equation to approximate liquid injectivity in a SAG process (Leeftink, Latooij, & Rossen, 2015). However, based Gong et al. (2018), there is a large discrepancy between the radial-flow model and finite-difference simulations in which the well pressure is estimated using the Peaceman equation. This indicates that these conventional simulations drastically underestimate gas and liquid injectivity in a 100 x 100 meter grid block (Gong et al., 2018).

This paper builds upon the research recently conducted by Gong et al. The main focus of the simulations is to determine how grid refinement affects liquid and gas injectivity. Ultimately, this paper seeks to determine the differences between using a coarse grid and using refined grids.

Chapter 2 covers theory and background information, as well as summarizing the highlights of Gong et al.'s paper. In Chapter 3, the methodology of the modelling and simulation is explained. Chapter 4 includes the discussion and results of the simulation model. The paper concludes in Chapter 5 with an overall summary and future recommendations.

2

Background and Theory

2.1. Gong et al.'s Summary of Results

2.1.1. Gong et al.'s Laboratory Experiment

Gong et al. (2018) conducted a series laboratory experiments to reflect gas and liquid injectivity in the nearby well region during the SAG process. During the core-flood experiments, foam was injected into a Berea core, and pressure differences were measured across the core. Directly after foam injection, liquid injectivity was examined, followed by extended periods of gas injection. Based on these experiments, Gong et al. concluded that injectivity during a SAG process is affected by the propagation of several uniform banks. Figure 1 below displays the banks that form during gas injection, whereas Figure 2 displays the banks that form during liquid injection.

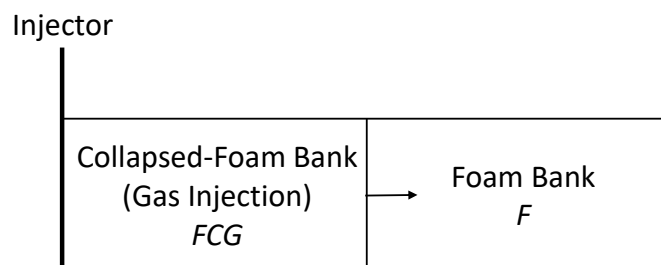


Figure 1. Gas injection foam banks (Gong et al., 2018).

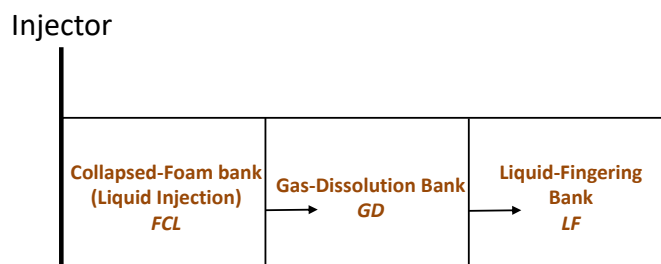


Figure 2. Liquid injection banks (Gong et al., 2018).

The collapsed-foam bank is a region of significantly weakened foam that slowly propagates from the inlet. The liquid-fingering bank forms as liquid fingers after the liquid has saturated the collapsed-foam bank. Gas dissolves within the liquid-fingering bank, forming the gas dissolution bank (Gong et al., 2018).

2.1.2. Linear-flow Model

Based on the experimental results, a linear-flow model was implemented using Darcy's Law for multi-phase flow:

$$\Delta p = \sum \Delta p_b \quad (1)$$

$$\Delta p_b = \int_{l_1}^{l_2} \frac{Q_t}{A \lambda_t(b)} dl = \frac{Q_t}{A} \frac{(l_2 - l_1)}{\lambda_t(b)} \quad (2)$$

where:

- Δp = total pressure difference
- Δp_b = pressure difference of a bank
- l_1 = starting position of the bank
- l_2 = ending position of the bank
- $\lambda_t(b)$ = total mobility of the bank
- Q_t = volumetric flow rate
- A = cross-sectional area

It was assumed that the total mobility throughout each bank was uniform and that the total pressure difference is equal to the summation of pressure differences of each individual foam bank. Figure 3 and Figure 4 below compares the laboratory results to the linear-flow model. Overall, the fit is within reason.

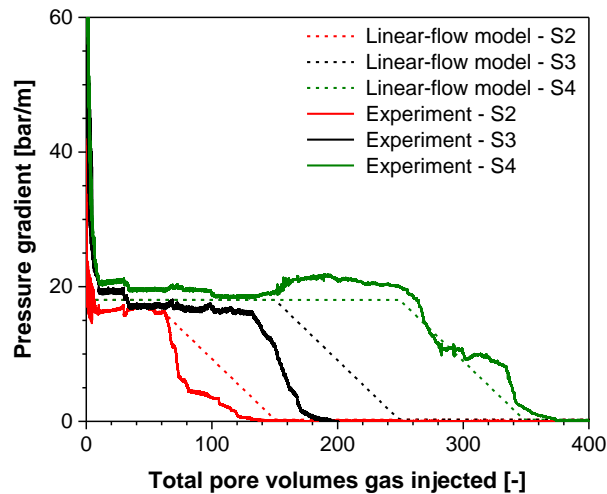


Figure 3. Pressure gradient comparison during gas injection (Gong et al., 2018).

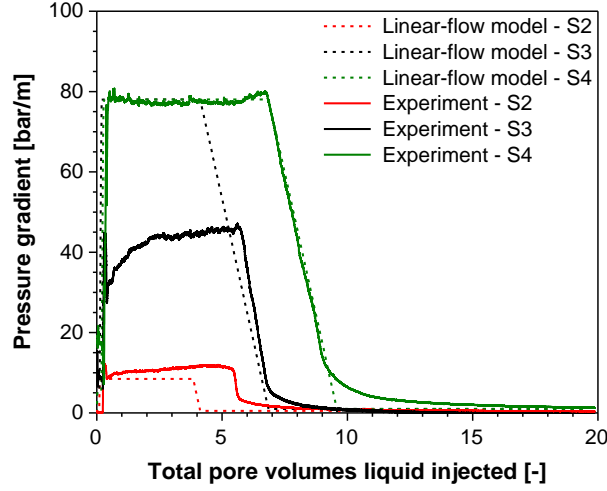


Figure 4. Pressure gradient comparison during liquid injection following 135 TPV of gas injection (Gong et al., 2018).

2.1.3. Radial-flow Model

Subsequently, a radial-flow model was created based off the core-flood experiment's results. For each bank, the pressure differences were calculated through Darcy's radial flow equation:

$$\Delta p_b = \int_{r_1}^{r_2} \frac{Q_t}{2\pi r h \lambda_t(b)} dr = \frac{Q_t}{2\pi r h} \frac{1}{\lambda_t(b)} \ln\left(\frac{r_2}{r_1}\right) \quad (3)$$

where r_1 and r_2 are the radial endpoints of the bank.

2.1.4. Conventional Foam Simulation

Foam simulations have conventionally been done through population-balance models or implicit-texture (IT) models (Cheng et al., 2000; Kam et al., 2007). Population-balance models recreate the formation and destruction of lamellae in order to determine its effect on gas mobility (Kam et al., 2007). IT models use a mobility-reduction factor to reflect the decrease in gas mobility due to foam (Cheng et al., 2000; Renkema & Rossen, 2007). Gong et al. uses the IT foam model in order to calculate the dimensionless pressures during gas and liquid injection in a SAG process. To calculate injectivity, conventional foam simulation models use the Peaceman equation.

2.1.5. The Peaceman Equation

As stated previously, many conventional reservoir simulators use the Peaceman equation to calculate the differential pressure between a well and its grid block. Using finite difference methods, Peaceman provided some of the first theoretical well equations for single-phase flow on square grids (Chen & Zhang, 2009). One of the main takeaways of Peaceman's work is that the calculated block pressure is related to the well's actual steady-state pressure at a given radius (r_e). Using an analytical approach, a numerical approach and a system of difference equations to derive r_e for a square grid, Peaceman concluded that $r_e \approx 0.2L$, where L is the length of the square grid (Chen & Zhang, 2009). While Peaceman's finite difference models have extended beyond square grids to include rectangular grids, non-

centered wells, anisotropic reservoirs and more, our simulations will solely incorporate square grids.

2.1.6. Gong et al.'s Assumptions

In order to simplify the model based on the Peaceman equation, Gong et al. made the following assumptions for the region of interest:

- Water and gas are the only fluids present
- All fluids are nearly incompressible
- The rock is nearly incompressible
- The reservoir's height is uniform
- The effect of gravity is ignored
- Viscous fingering and dispersion are disregarded
- Foam instantaneously reaches local equilibrium
- The grid block is fully saturated with water and surfactant before gas injection
- Water saturation is always uniform

2.1.7. Comparison between Radial-flow Model and Peaceman Equation

When Gong et al. compared the radial-flow model to the Peaceman equation with the STARS foam model, they found that the Peaceman equation model severely underestimates gas and liquid injectivity for a 100 by 100 meter grid block. Figure 5 and Figure 6 below display dimensional pressure drops calculated from the Peaceman equation and the radial-flow model.

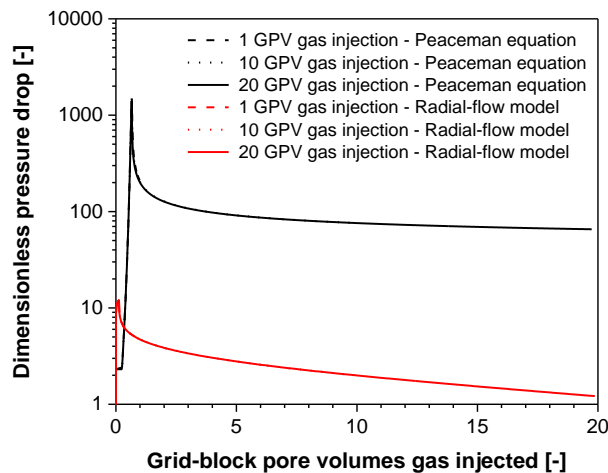


Figure 5. Dimensionless pressure drop during gas injection for Peaceman equation and radial-flow model (Gong et al., 2018).

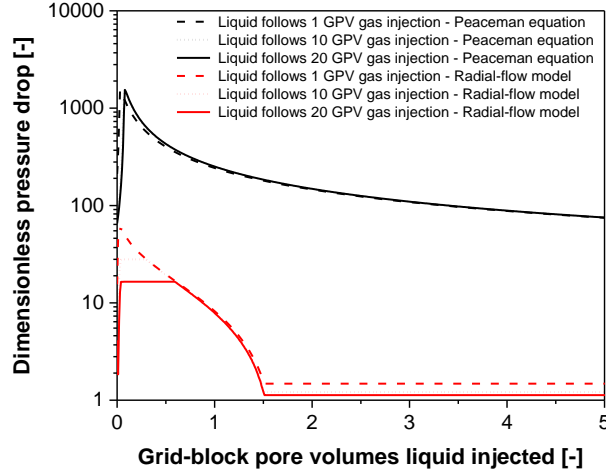


Figure 6. Dimensionless pressure drop during liquid injection for Peaceman equation and radial-flow model (Gong et al., 2018).

There is a large discrepancy between the radial-flow model and the calculations based on the Peaceman equation. Gong et al. concluded that the Peaceman equation drastically underestimates gas and liquid injectivity. A skin factor could be used to roughly bridge the gap between the Peaceman equation and the radial-flow model (Gong et al., 2018).

Our simulation models will test how grid refinement impacts liquid and gas injectivity. In addition, our simulations will provide the foundation for determining whether grid refinement is a major reason for the discrepancy between the radial-flow model and the Peaceman equation model or whether most of the error comes from an incorrect model. When a block size is much larger than the well size, the reservoir simulator's calculation of block pressure may not be a good representation of the well pressure (Abou-Kassem & Aziz, 1985). Thus, by refining the grid, it may be possible to determine whether the Peaceman equation actually underestimates liquid and gas injectivity during SAG processes.

2.2. STARS Foam Modelling

In order to simulate the reduction in gas relative permeability due to foam, the STARS model utilizes a foam mobility reduction factor (FM):

$$k_{rg}^f = k_{rg}(S_w) * FM \quad (4)$$

This reduction factor is calculated using the equation:

$$FM = \frac{1}{1 + fmmob * F_1 F_2 F_3 F_4 F_5 F_6} \quad 0 \leq F_i \leq 1 \quad (5)$$

where:

- $fmmob$ = the reference gas-mobility-reduction factor of wet foams
- F_1 = surfactant concentration effect
- F_2 = water saturation effect

- F_3 = oil saturation effect
- F_4 = gas velocity effect
- F_5 = capillary number effect
- F_6 = critical capillary number effect

For this study, F_2 will be the only function that is taken into account. The simplified equation is now:

$$FM = \frac{1}{1 + fmmob * F_2} \quad (6)$$

The F_2 function is represented by the equation below:

$$F_2(S_w) = 0.5 + \frac{\arctan[epdry \cdot (S_w - fmdry)]}{\pi} \quad (7)$$

where:

- $epdry$ = the parameter that controls the abruptness of the foam's transition from low-quality to high-quality regime
- $fmdry$ = the water saturation at the foam's transition point

The F_5 function models the shear-thinning behaviour observed in the low quality regime through the following two parameters: $epcap$ which is related to the power-law exponent and a parameter set to the smallest expected capillary number, known as $fmcap$ (Boeije & Rossen, 2015; Rossen & Boeije, 2013). However, since this paper does not focus on the effects of shear-thinning, $epcap$ and $fmcap$ are neglected in the foam model.

3

Methodology

3.1 The Grid Models

The base case is performed on a 5x5x1 grid with four producing wells in the corner and one injection well in the center, as seen in Figure 7. The reservoir is initially completely filled with water ($S_{wi} = 1$). Each grid block is 20 meters long, 20 meters wide, and 10 meters thick.

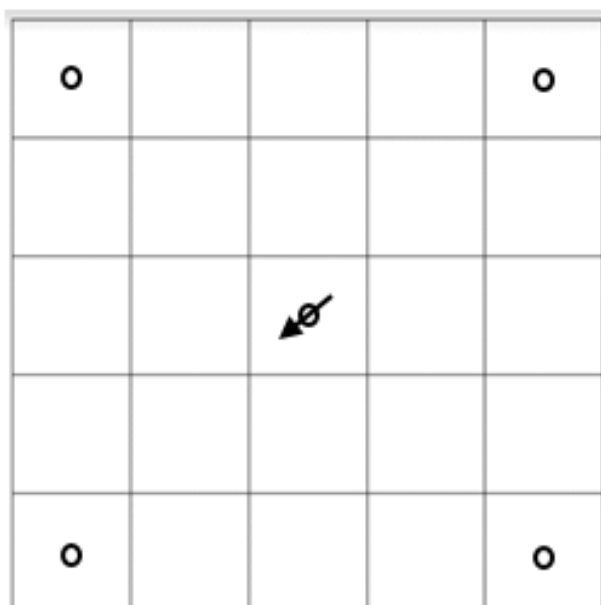


Figure 7. Base case: 5x5x1 grid

There are two refined grid scenarios. The first refined layout is displayed in Figure 8, where the center grid block is now partitioned into 9 equal parts. The second refined layout is shown in Figure 9, where the center block is split into 25 equal parts.

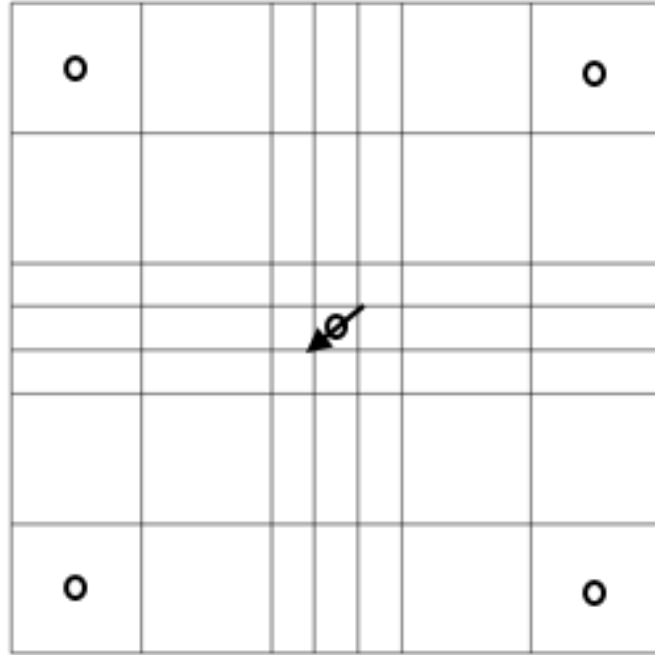


Figure 8. Refined grid: 3x3 Center

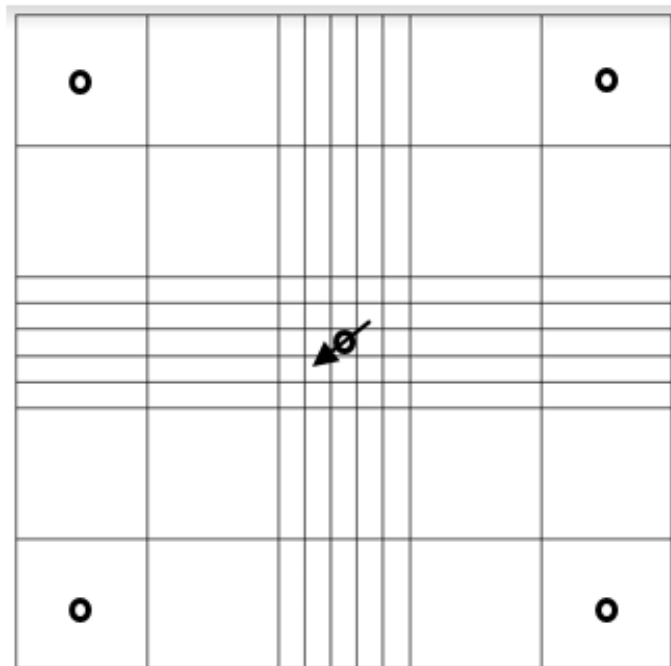


Figure 9. Refined grid: 5x5 Center

3.2 General Parameters

One of Gong et al.'s assumptions is that all fluids are virtually incompressible. The STARS simulator, however, always considers gaseous components to be compressible. In order to minimize the effects of gas compression, we set the initial reservoir pressure to 100 bar (1450.38 psi), injected the nitrogen gas at a low rate of 800 m³/day (28,251.7 ft³/day) and extended the time period in which the nitrogen gas was injected. In general, the gas

expansion was calculated to be around 36.5 %. Although this does not completely eliminate gas compressibility, it does lower its overall effect. Other parameter values, such as well radius, porosity and permeability, were taken from Gong et al.'s paper. Table 1 lists these values.

Table 1. CMG STARS Array Properties

Parameter	Value
Porosity	0.2
Permeability	150 mD
$S_{w,initial}$	1
$S_{o,initial}$	0
$S_{g,initial}$	0
Initial Pressure	10,000 kPa
Well Radius	0.1 m
Δt	1 day

Additionally, we set one individual grid block to be equivalent to one pore volume. The timeline of our simulation for each grid case starts with an initial injection of surfactant at 1000 m³/day for 20 days to fill the entire grid with surfactant (25 PV injected). For the next 500 days, nitrogen gas was injected at 800 m³/day (5 PV injected). For the next 2500 days, surfactant was reinjected into the reservoir at a rate of 1.6 m³/day (5 PV injected). The temperatures of the surfactant and gas were kept at 20 °C. All four of the producer wells were kept at an operating bottom-hole pressure of 10,000 kPa (100 bar).

3.3 Relative Permeability Parameters

STARS uses the Stone's Method to calculate phase relative permeability, which functions under the assumption that three phases are present in the model. However, since the initial oil saturation of the reservoir was set to zero, gas and water flow can be simulated. Table 2 displays the input values used to develop the relative permeability curves of water and gas.

Table 2. STARS Relative Permeability Parameters

SWCON - Endpoint Saturation: Connate Water	0.204
SWCRIT - Endpoint Saturation: Critical Water	0.204
SOIRW - Endpoint Saturation: Irreducible Oil for Water-Oil Table	0.25
SORW - Endpoint Saturation: Residual Oil for Water-Oil Table	0.25
SOIRG - Endpoint Saturation: Irreducible Oil for Gas-Liquid Table	0
SORG - Endpoint Saturation: Residual Oil for Gas-Liquid Table	0
SGCON - Endpoint Saturation: Connate Gas	0.25
SGCRIT - Endpoint Saturation: Critical Gas	0.25
KROCW - Kro at Connate Water	0.5
KRWIRO - K _{rw} at Irreducible Oil	0.14
KRGCL - K _{rg} at Connate Liquid	0.47
KROGCG - K _{rog} at Connate Gas	N/A
N_w - Exponent for calculating K _{rw} from KRWIRO	5.25
N_{ow} - Exponent for calculating K _{row} from KROCW	5
N_{og} - Exponent for calculating K _{rog} from KROGCG	5
N_g - Exponent for calculating K _{rg} from KRGCL	1.22

3.4 Foam Parameters

The foams parameters were based off Gong et al.'s experimental foam scan. The measurements are listed in Table 3 and the foam apparent viscosity is plotted against the foam gas fraction in Figure 10.

Table 3. Gong et al.'s foam scan measurements (Gong et al., 2018)

Foam gas fraction	Foam Apparent Viscosity (cp)
0.082436	225.06
0.169416	252.79
0.258021	282.27
0.339653	315.54
0.345169	309.56
0.440494	331.51
0.528534	377.71
0.530925	377.38
0.634956	396.54
0.748817	403.02
0.809117	399.45
0.876698	328.89
0.989656	69.4

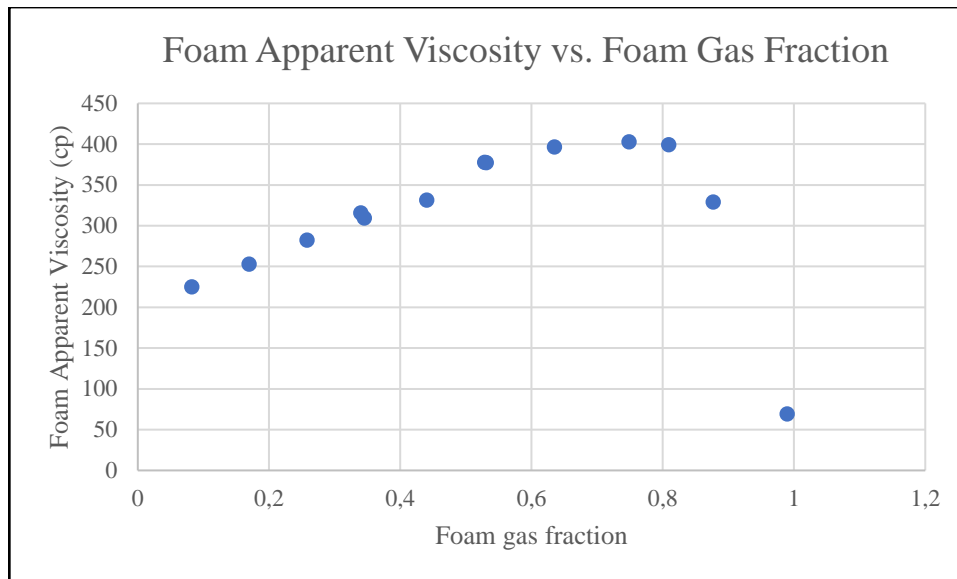


Figure 10. Foam Apparent Viscosity vs. Foam Gas Fraction (Gong et al., 2018).

The foam parameters used in the STARS simulation are listed in Table 4 below. The foam model does not include shear thinning parameters (*epcap* and *fmcap*), so the foam parameters do not completely match the parameters listed in Gong et al.’s paper. The Newtonian foam parameters listed below were obtained from Jiakun Gong in person.

Table 4. Foam Parameters

Parameter	Value
<i>fmdry</i>	0.35
<i>epdry</i>	320
<i>fmmob</i>	5.14×10^4

One important thing to note is that STARS’s Process Wizard uses *sfdry* and *sfbet* to denote *fmdry* and *epdry* respectively.

4

Results

4.1 Dimensionless Pressure

After the pressure data points were extracted, dimensionless pressure was calculated so that they may be compared with Gong et al.'s results. For the original 5x5x1 grid, the formula for dimensionless pressure is:

$$P_D = \frac{(P_w - P_i)_{w+g}}{(P_w - P_i)_w} * \frac{Q_w}{Q_{w+g}} \quad (8)$$

where:

- P_w = actual well pressure
- P_i = grid-block pressure
- $()_w$ = initial surfactant injection
- $()_{w+g}$ = injection of water and/or gas after initial injection of surfactant
- Q_w = initial rate of surfactant injection
- Q_{w+g} = rate of water and/or gas injection after initial injection of surfactant

For the original grid, the dimensionless pressure was calculated from Equation 8 and then plotted against the pore volumes (PV) injected. Figure 11 and

Figure 12 show the results for dimensionless pressure drop after injecting gas and liquid following SAG for the unrefined grid.

For the refined grids, we took an average pressure of all the central refined blocks and set that as the well block pressure of the center grid block. Afterwards, the resulting dimensionless pressure drop was plotted versus PV injected. Figure 13 and Figure 14 show the dimensionless pressure drops when the center grid was refined to a 3x3 grid, and Figure 15 and Figure 16 show the pressure drops when the center grid was refined to a 5x5 grid.

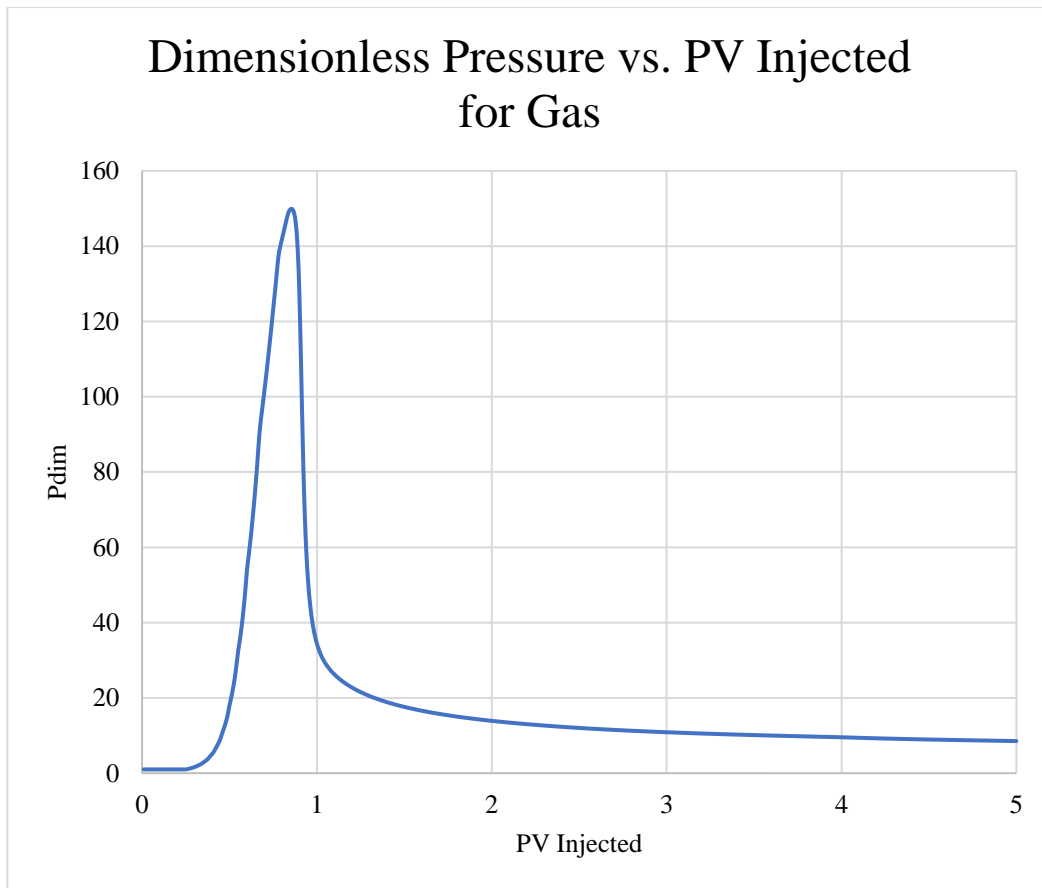


Figure 11. Original Grid: Dimensionless Pressure vs. PV Injected after gas injection

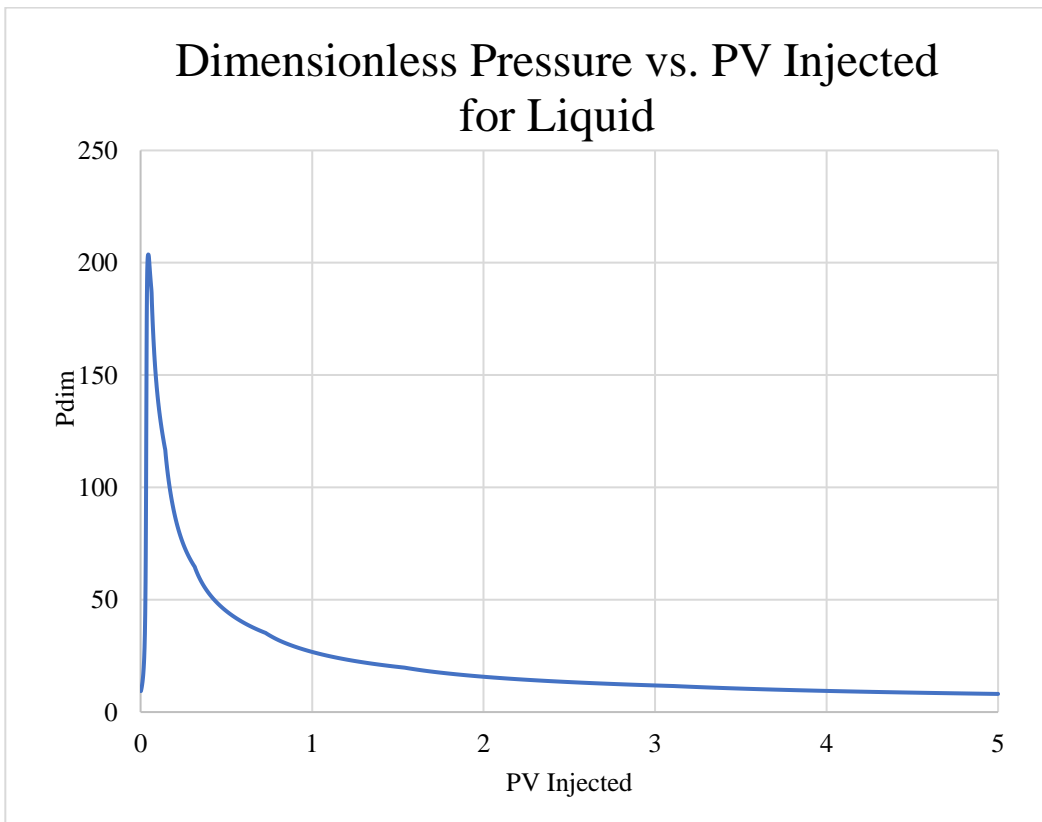


Figure 12. Original Grid: Dimensionless Pressure vs. PV Injected after liquid injection

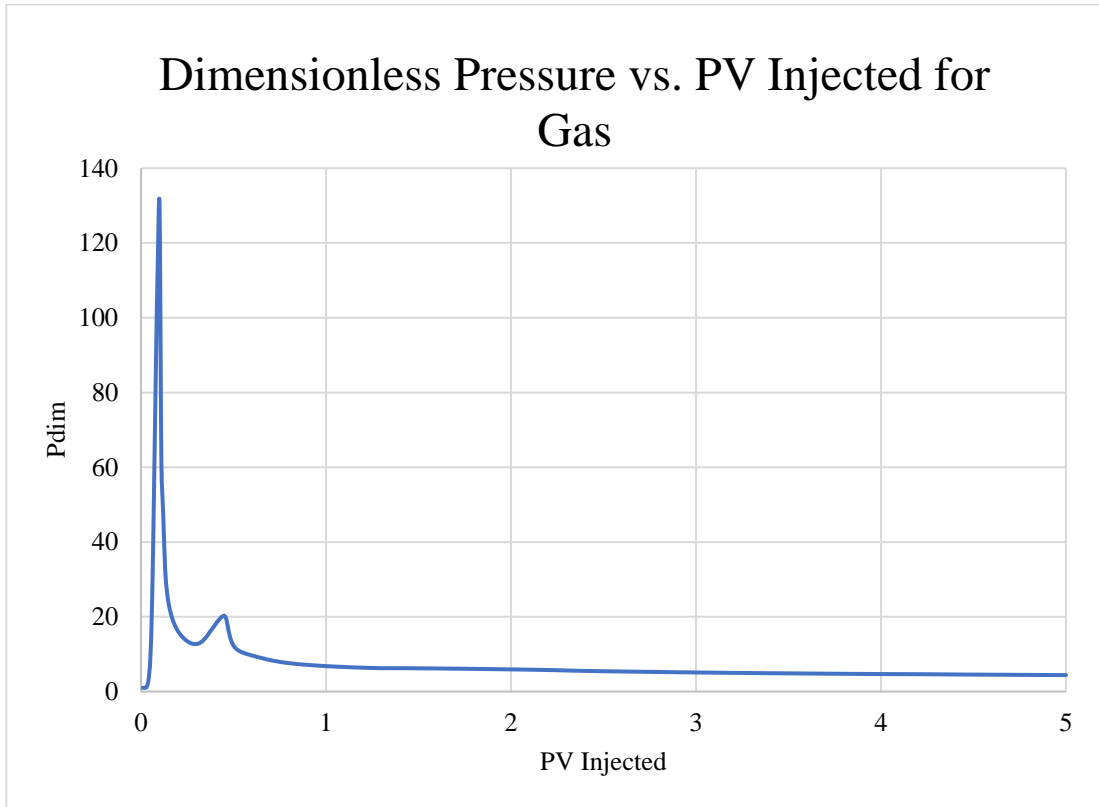


Figure 13. Refined 3x3 Grid: Dimensionless Pressure vs. PV Injected after gas injection

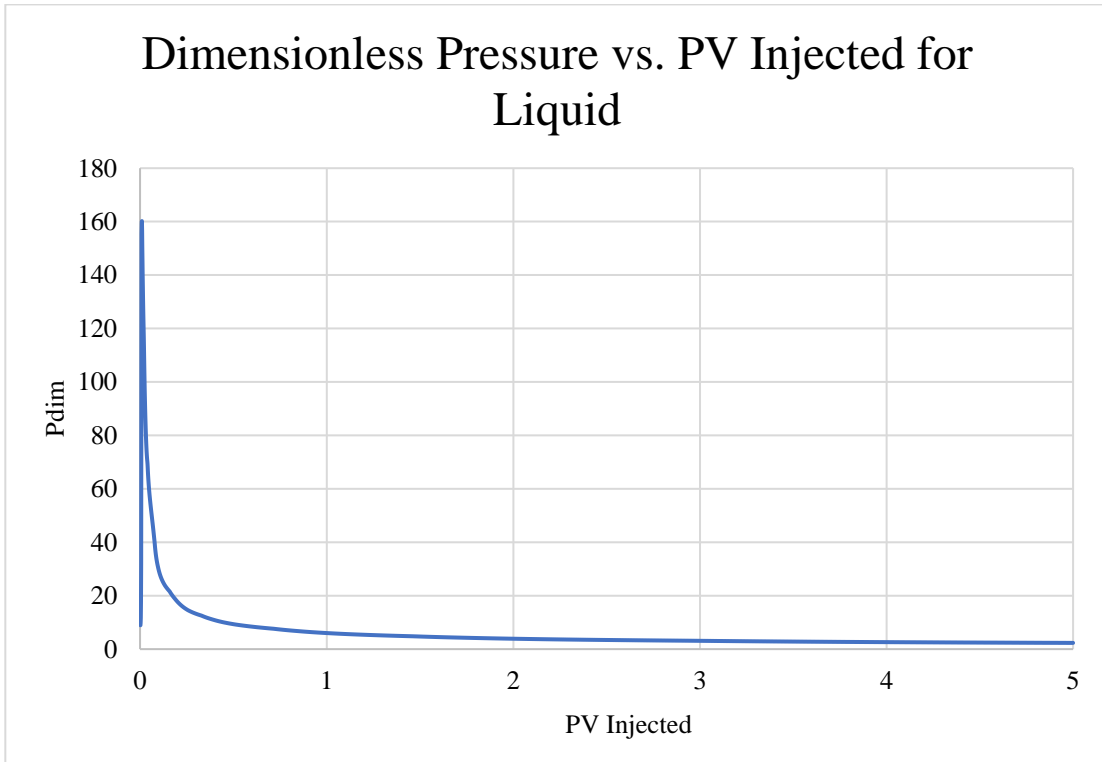


Figure 14. Refined 3x3 Grid: Dimensionless Pressure vs. PV Injected after liquid injection

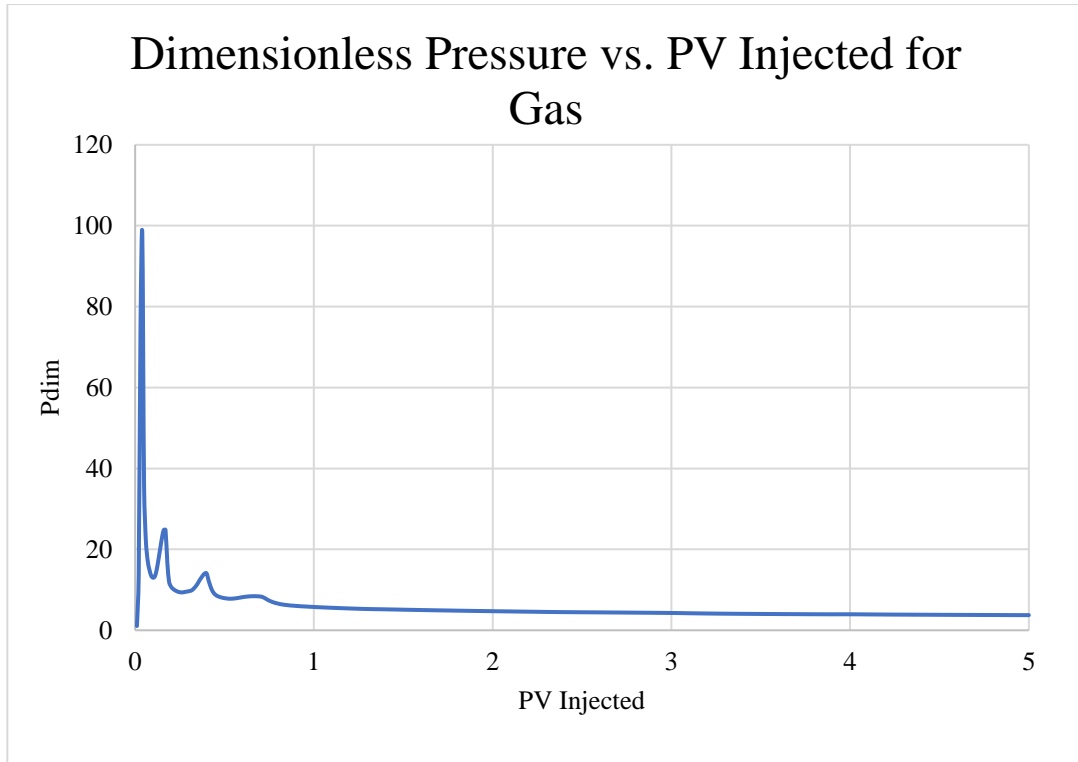


Figure 15. Refined 5x5 Grid: Dimensionless Pressure vs. PV Injected after gas injection

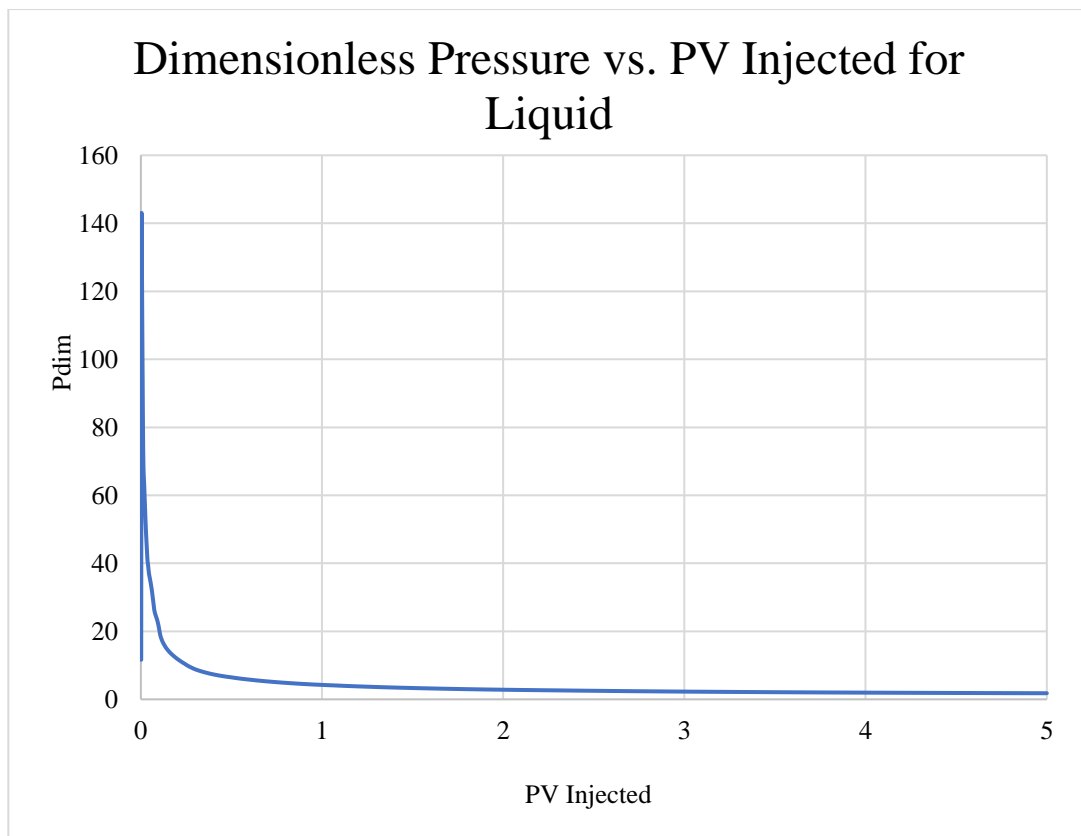


Figure 16. Refined 5x5 Grid: Dimensionless Pressure vs. PV Injected after liquid injection

4.2 Comparison of Pressures along the Grid's Diagonal

For each grid scenario, the pressures along the diagonal of the grid were also plotted against PV injected in order to compare the evolution of the well block pressures across the grid. Figure 17 displays the specific grid blocks in which we plotted the well block pressures for the refined 5x5 grid scenario. The main center grid block is set to be P1, and the refined grid pieces within the P1 block are denoted as P1a, P1b and P1c.

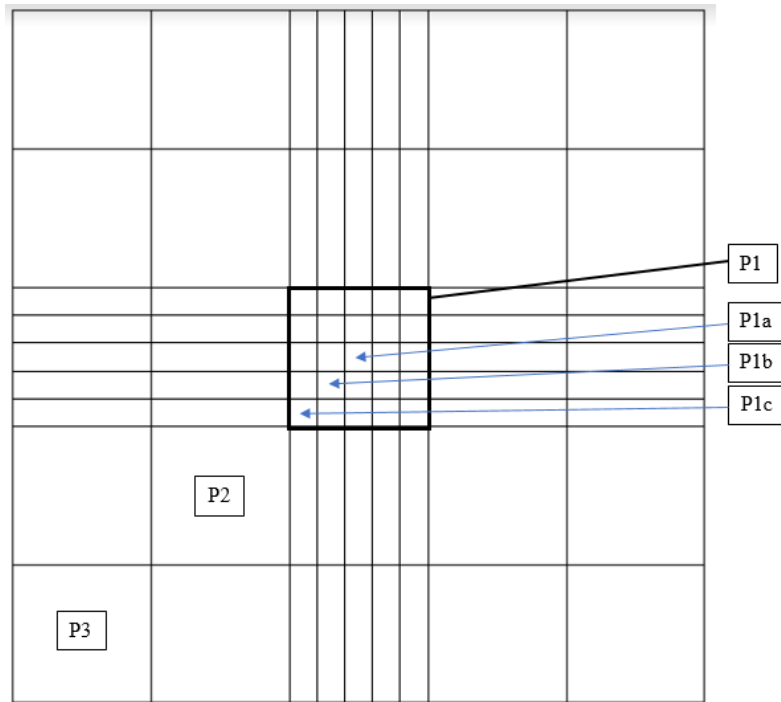


Figure 17. Pressure notation along the grid block diagonal

The well and well block pressures for the initial surfactant injection phase is shown in Table 5. Figure 18 through Figure 23 are graphs that display the well and well block pressures during gas and liquid injection for the original grid and the refined grids.

Table 5. Diagonal Pressure Values during Initial Water Injection

Grid Refinement	Pwf of Injection well (kPa)	P1 (kPa)			P2 (kPa)	P3 (kPa)	Pwf of Production well (kPa)
		P1a	P1b	P1c			
Original	20528.49	15623.93			12901.49	11226.14	10000.00
Refined 3x3	20711.69	17271.81	14565.30	N/A	12913.69	11226.14	10000.00
Refined 5x5	20723.56	17964.71	15292.59	14361.02	12915.03	11226.14	10000.00

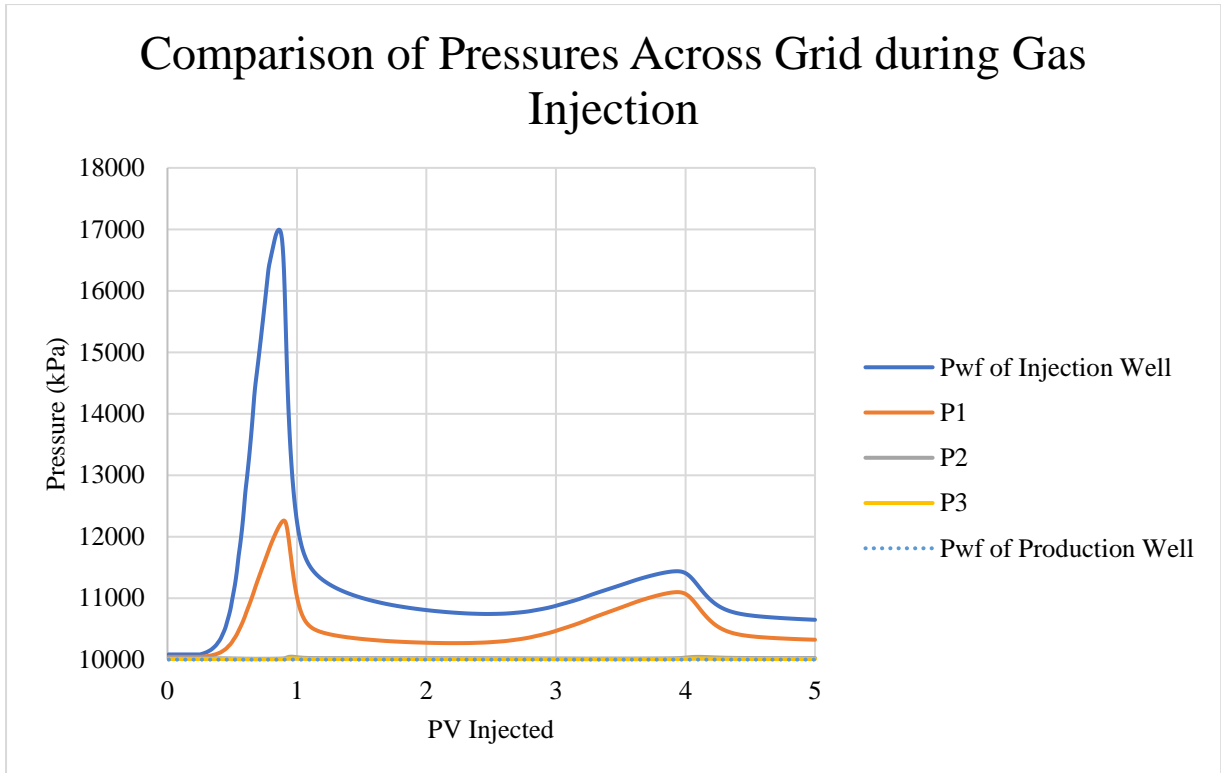


Figure 18. Original Grid: Diagonal pressures during gas injection

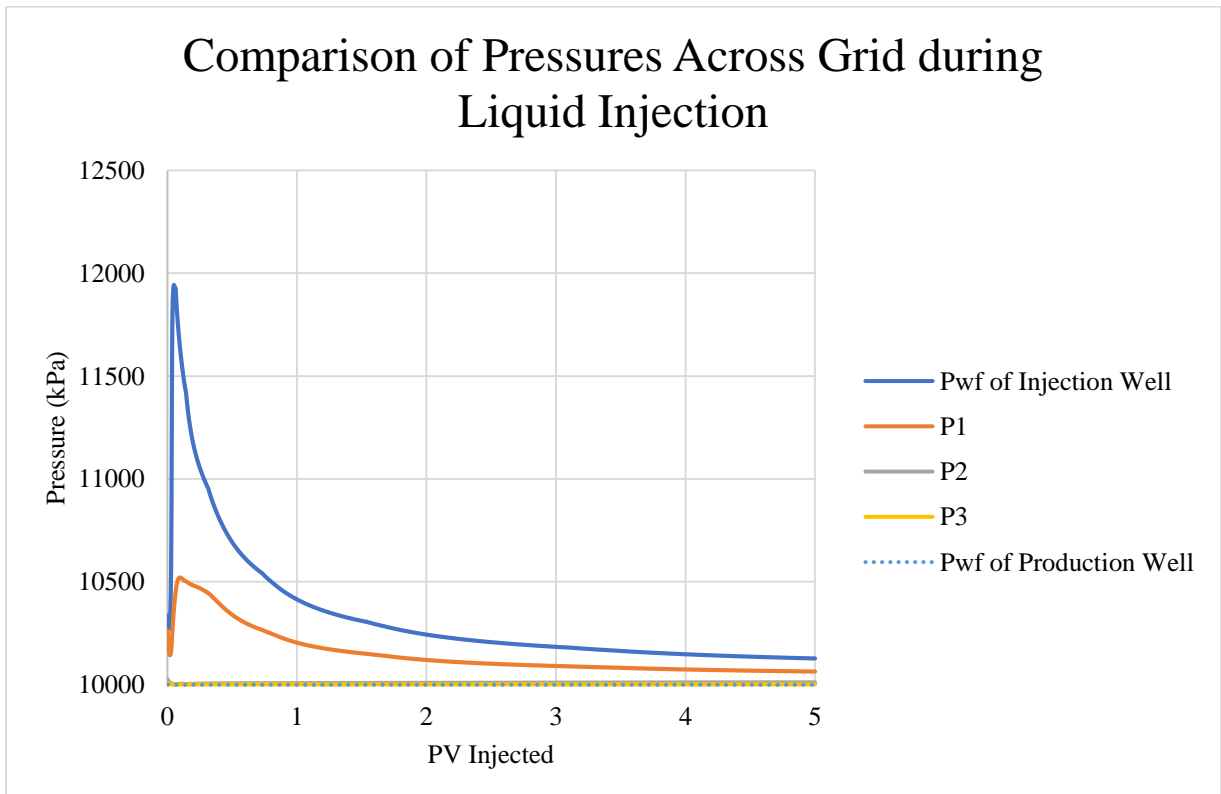


Figure 19. Original Grid: Diagonal pressures during liquid injection

Comparison of Pressures Across Grid during Gas Injection

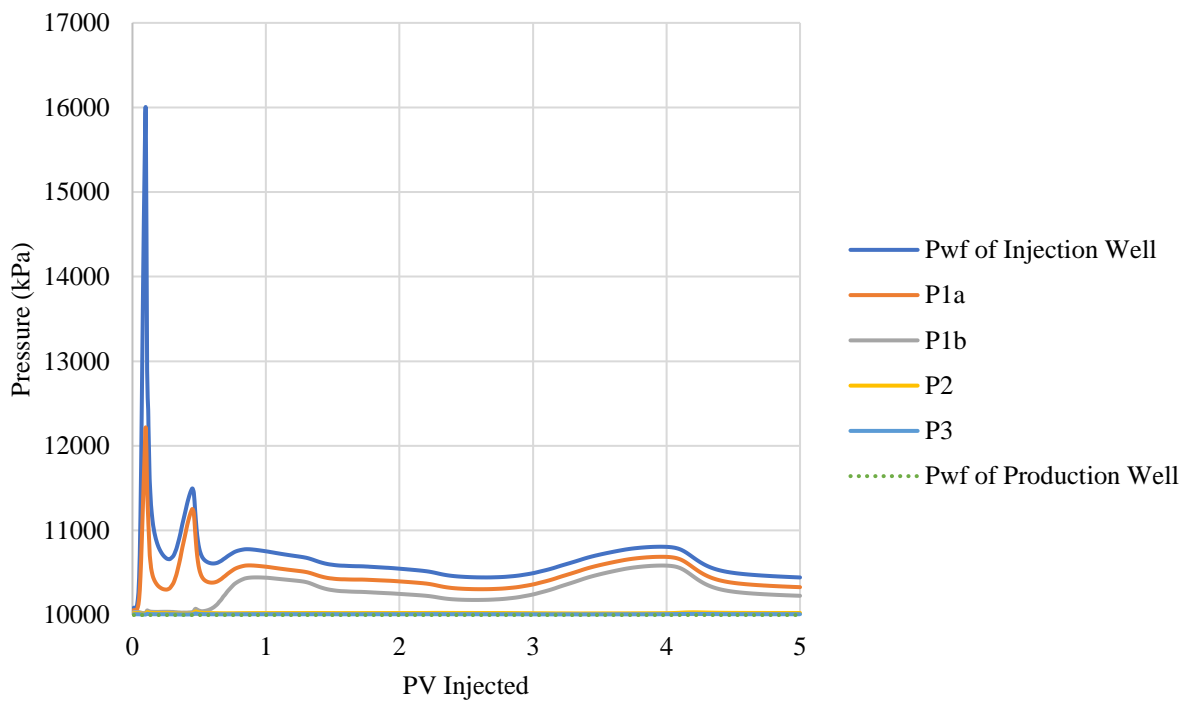


Figure 20. Refined 3x3 Grid: Diagonal pressures during gas injection

Comparison of Pressures Across Grid during Liquid Injection

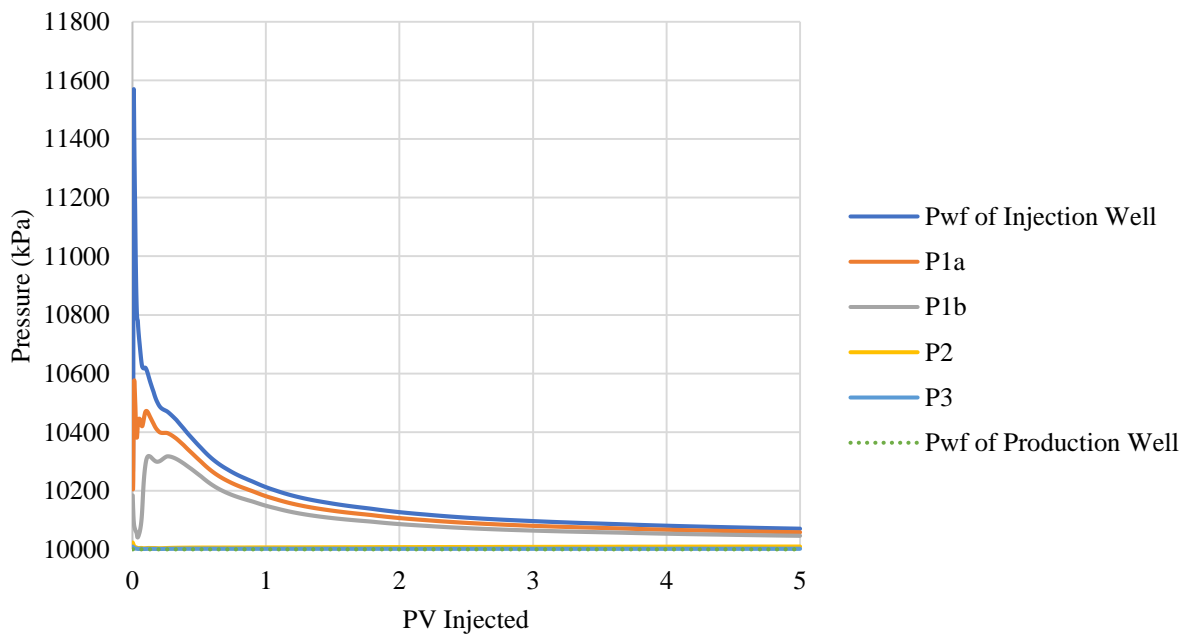


Figure 21. Refined 3x3 Grid: Diagonal pressures during liquid injection

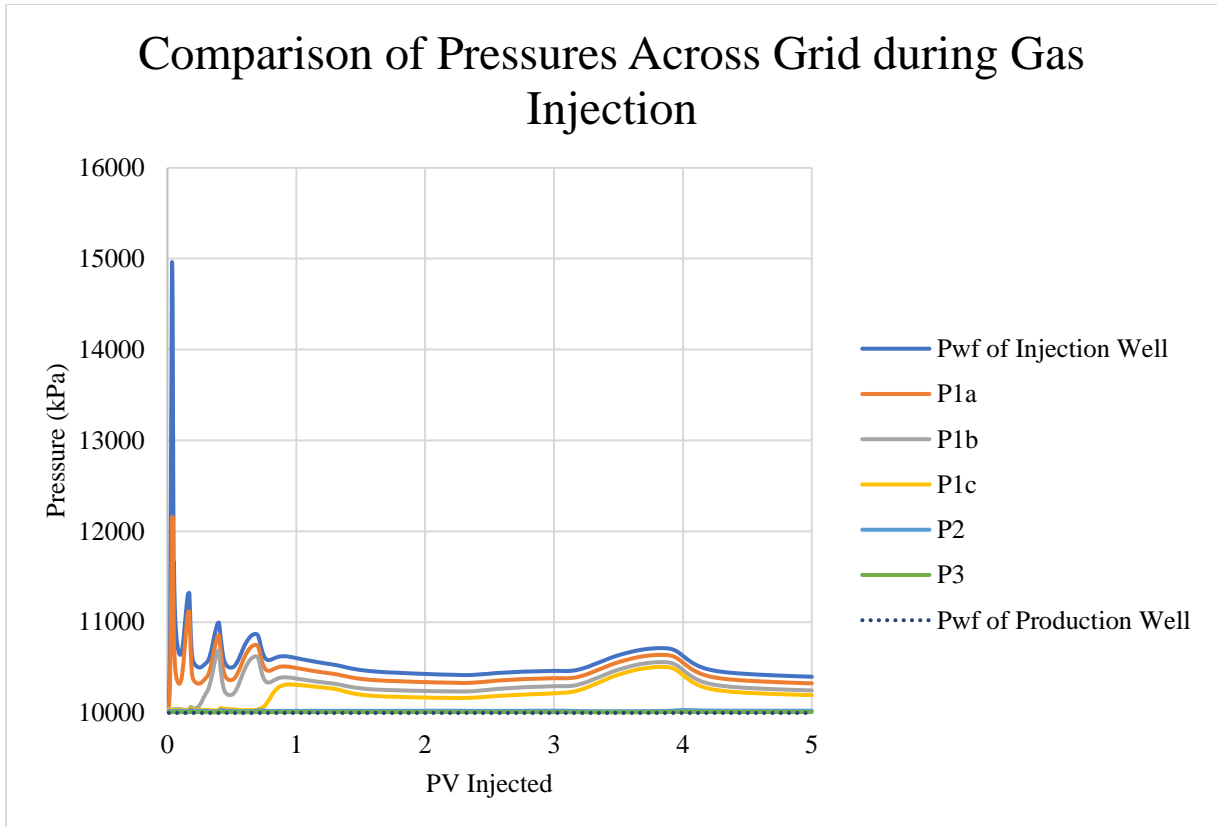


Figure 22. Refined 5x5 Grid: Diagonal pressures during gas injection

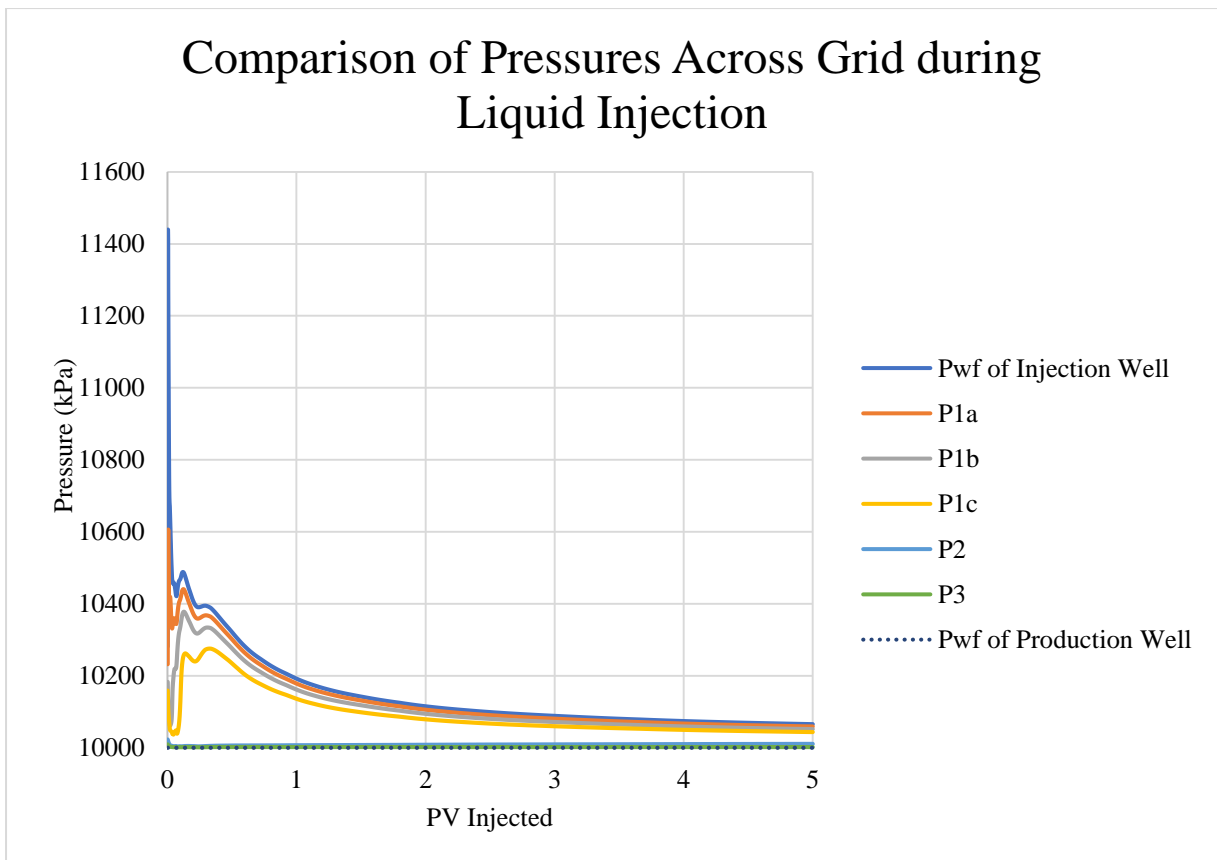


Figure 23. Refined 5x5 Grid: Diagonal pressures during liquid injection

5

Conclusion and Recommendations

The results of the STARS simulations indicate that grid refinement does have a notable impact on how quickly the pressure drop occurs. Based on the results, the dimensionless pressure drops significantly faster once the grid has been refined. We observed that the pressure drop occurs approximately 9 times faster for the 3x3 refined grid scenario when compared to the base grid case. For the 5x5 refined grid scenario, the pressure drop occurs 25 times faster than that of the original grid case. The magnitude of the initial pressure peak also slightly decreases as the grid is refined. The 3x3 refined grid and the 5x5 grid case saw a decrease of 24.6 % and 29.7 % respectively in the pressure peak's magnitude when compared to that of the base grid. In the refined cases, we also see smaller peaks in pressure after the initial pressure drop. This is likely correlated to each time a drop in relative mobility occurs in a new grid block, which is further confirmed by our comparison the pressures of various grid blocks along the diagonal of the grid. Ultimately, our results indicate that grid refinement improves gas and liquid injectivity. Since we did not use the exact same parameters as Gong et al., we cannot quantify how much of the discrepancy is due to grid refinement and how much of the discrepancy is due to using a coarse grid. Despite this, we do not expect grid refinement to completely eliminate the discrepancy observed by Gong et al. because the model based on Peaceman's equation does not take all of the foam banks into account.

There are a few main points to consider for future research. First, our simulations utilized a time step of 1 day, but as a future recommendation, it may be better to reduce the time step to 1 hour or 1 minute during the time period in which the relative mobility drops. Decreasing the time step of the iterations around the region of pressure drop could help provide better accuracy and clarity, especially since we have observed that the pressure drop occurs much faster once the grid has been refined. Second, for the refined grids, we took an average pressure of all the central refined blocks and set that as the well block pressure of the center grid block. For future references, it would be important to find the best way to represent the well-block pressure of the center grid block once the grid has been refined. Additionally, it would be helpful to develop a method to convert the pressures across the diagonal of the grid to dimensionless pressures. Lastly, it would be important to compare the simulation's results with the fractional-flow theory to confirm whether the Peaceman equation still significantly underestimates gas and liquid injectivity during SAG foam EOR.

References

- Abou-Kassem, J. H., & Aziz, K. (1985). Analytical Well Models for Reservoir Simulation. *Society of Petroleum Engineers Journal*, 25(4), 573–579. <https://doi.org/10.2118/11719-PA>
- Boeije, C. S., & Rossen, W. R. (2015). Fitting Foam-Simulation-Model Parameters to Data : I . Coinjection of Gas and Liquid. *SPE Reservoir Evaluation & Engineering*, 18(February), 264–272. <https://doi.org/10.2118/174544-PA>
- Chen, Z., & Zhang, Y. (2009). Well Flow Models for Various Numerical Methods. *International Journal of Numerical Analysis and Modeling*, 6(3), 375–388.
- Cheng, L., Reme, A. B., Shan, D., Coombe, D. A., & Rossen, W. R. (2000). Simulating Foam Processes at High and Low Foam Qualities. In *SPE/DOE Improved Oil Recovery Symposium*. Society of Petroleum Engineers. <https://doi.org/10.2118/59287-MS>
- Gong, J., Vincent-Bonnieu, S. V., Bahrim, R. Z., Petronas, J., Groenenboom, R., & Farajzadeh. (2018). Modelling of Liquid Injectivity in Surfactant-Alternating-Gas Foam Enhanced Oil Recovery. *Society of Petroleum Engineers*.
- Kam, S. I., Nguyen, Q. P., Li, Q., & Rossen, W. R. (2007). Dynamic Simulations With an Improved Model for Foam Generation. *SPE Journal*, 12(1), 35–48. <https://doi.org/10.2118/90938-PA>
- Lake, L. W. (1989). *Enhanced Oil Recovery*. Englewood Cliffs, N.J: Prentice Hall.
- Leeftink, T. N., Latooi, C. A., & Rossen, W. R. (2015). Injectivity errors in simulation of foam EOR. *Journal of Petroleum Science and Engineering*, 126, 26–34. <https://doi.org/10.1016/j.petrol.2014.11.026>
- Renkema, W. J., & Rossen, W. R. (2007). Success of SAG Foam Processes in Heterogeneous Reservoirs. *Society of Petroleum Engineers*.
- Rossen, W. R. (1996). Foams in Enhanced Oil Recovery. In R. K. Prud'homme & S. A. Khan (Eds.), *Foams: Theory: Measurements: Applications* (pp. 413–464). New York: Marcel Dekker Inc.
- Rossen, W. R., & Boeije, C. S. (2013). Fitting Foam Simulation Model Parameters for SAG Foam Applications. In *SPE Enhanced Oil Recovery Conference* (Vol. 2, pp. 2–4). Society of Petroleum Engineers. <https://doi.org/10.2118/165282-MS>

Shan, D., & Rossen, W. (2002). Optimal Injection Strategies for Foam IOR. In *SPE/DOE Improved Oil Recovery Symposium*. Society of Petroleum Engineers. <https://doi.org/10.2118/75180-MS>

Terry, R. E. (2003). Enhanced Oil Recovery. In *Encyclopedia of Physical Science and Technology* (Vol. 18, pp. 503–518). Elsevier. <https://doi.org/10.1016/B0-12-227410-5/00868-1>